International Journal of Urban Management and Energy Sustainability (IJUMES)

Homepage: http://www.ijumes.com

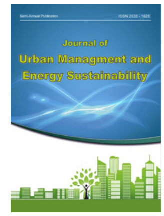

CASE STUDY RESEARCH PAPER

Assessing Urban Thermal Vulnerability Using GIS and Multi-Criteria Decision-Making for Climate Change Adaptive Planning (Case Study: Tabriz City, Iran)

Farhad Faghihi*[1], Seyed Hossein Yousefianvar[2]

*1*Department of Civil Engineering, Technical and Vocational University (TVU), Tehran, Iran*

2 Department of Architecture, Sav.C., Islamic Azad University, Saveh, Iran

ARTICLE INFO

Article History:
Received 2026-02-08
Revised 2026-04-22
Accepted 2026-05-28

Keywords:
Climate-change; Fuzzy AHP; Geographic Information Systems; thermal vulnerability; urban heat

DOI: 10.22034/ijumes.2026.738888

ABSTRACT

Rapid urbanization and climate change are intensifying urban heat, making the identification of heat-vulnerable areas essential for climate-adaptive planning. Guided by the IPCC framework, which defines vulnerability through exposure, sensitivity, and adaptive capacity, this study develops and demonstrates an integrated approach for assessing and mapping urban thermal vulnerability in Tabriz, a large semi-arid city in northwestern Iran with limited green space. The methodology integrates geographic information systems (GIS), multi-criteria decision-making, and social-science measurement. Twelve indicators were organized across the three vulnerability components. Real land-use data were processed in GIS, while residents' perceptions were assessed using a structured five-point Likert questionnaire administered to 384 respondents determined by the Cochran formula. An 18-member expert panel provided pairwise comparisons. Criterion weights were derived using the Fuzzy Analytic Hierarchy Process (Fuzzy-AHP), while exploratory and confirmatory factor analyses examined construct validity. Covariance-based structural equation modelling (SEM/LISREL) tested hypothesized relationships, and weighted overlay analysis generated a five-level Thermal Vulnerability Index (TVI) map, validated against summer land-surface temperature. The land-use analysis indicates that barren and abandoned land (35.4%), agriculture (19.1%), and residential fabric (17.2%) dominate Tabriz city, whereas green land uses comprise only 5.3% of the urban area. The demonstrative model indicates that exposure and sensitivity increase thermal vulnerability, while adaptive capacity reduces it and partially mediates the effect of exposure. Approximately 36% of the urban area falls within high or very-high vulnerability classes, primarily in dense built-up zones with limited green cover. The framework provides a transparent, reproducible, and transferable decision-support tool for prioritizing heat-adaptation interventions.

Running Title: Urban Thermal Vulnerability Using GIS and Multi-Criteria Decision-Making for Climate-Change

NUMBER OF REFERENCES	NUMBER OF FIGURES	NUMBER OF TABLES
35	13	09

*Corresponding Author:
Email: *Farhad.faghihi@ut.ac.ir*
Phone: +982166319882
ORCID: https://orcid.org/0000-0001-6817-5964

INTRODUCTION

Cities concentrate people, impervious surfaces and waste heat, and as a result they are typically several degrees warmer than their rural surroundings a phenomenon known as the urban heat island (UHI) (Deilami et al., 2018). Under accelerating climate change, the combination of a warming background climate and continued urban expansion is lengthening and intensifying periods of extreme urban heat, with well-documented consequences for human health, energy demand and outdoor comfort (Wu et al., 2022) (Rathi et al., 2022). Because heat does not affect all parts of a city equally, planners increasingly need spatially explicit information about where the most heat-vulnerable areas are, and why, so that limited adaptation resources can be directed to the places and populations that need them most (Inostroza et al., 2016). The dominant conceptual lens for such assessments is the vulnerability framework of the Intergovernmental Panel on Climate Change, in which vulnerability is understood as a function of three components: exposure (the degree to which a place experiences hazardous heat), sensitivity (the degree to which the people and fabric present are susceptible to harm) and adaptive capacity (the resources, green space, services, socio-economic means that mitigate harm) (Rathi et al., 2022) (Wu et al., 2022). Operationalizing these components spatially has become feasible through the growth of satellite thermal remote sensing, which supplies land-surface temperature (LST) as an exposure proxy (Ermida et al., 2020) (Amindin et al., 2021), and through geographic information systems (GIS), which allow heterogeneous indicator layers temperature, land cover, imperviousness, population, green space to be standardized and combined (Bokaie et al., 2016) (Ranagalage et al., 2018). A recurring difficulty is that these indicators are measured in different units and contribute unequally to vulnerability, so they cannot simply be added together. Multi-criteria decision-making (MCDM) resolves this by assigning defensible weights to each criterion before overlay. The Analytic Hierarchy Process (AHP) and its fuzzy extension are the most widely used weighting techniques in GIS-based environmental assessment, because they translate expert judgement into consistent numerical weights and can accommodate the imprecision inherent in such judgements (Truong et al., 2023) (Kılıç et al., 2022). GIS–MCDM couplings using AHP, Fuzzy-AHP and TOPSIS have been applied successfully to a range of spatial suitability and hazard problems (Kabir & Guha Thakurta, 2024) (Rincón et al., 2018) (Sahraei et al., 2023) (Tien Bui et al., 2019), and are readily transferable to thermal vulnerability.

Alongside the physical layers, the way residents and experts perceive heat risk and the adequacy of adaptive resources is itself informative, and social-science measurement models allow such perceptions to be captured and validated. Questionnaire-based studies analyzed through factor analysis and structural equation modelling (SEM) have been used to examine how environmental attributes shape perceived comfort, restorativeness and climate-adaptation awareness (Peng et al., 2021) (Chen et al., 2022) (Lenzholzer et al., 2020). Integrating a perception-based measurement model with a GIS–MCDM index strengthens an assessment in two ways: it provides an independent, statistically validated account of how exposure, sensitivity and adaptive capacity relate to overall vulnerability, and it grounds the criterion set in the lived experience of the population at risk. Tabriz city, the largest city of north-western Iran, is an instructive case. Located on a semi-arid plateau, it experiences hot, dry summers, and as the land-use analysis below shows combines a very large share of barren and built-up land with a strikingly small green-space endowment. Studies of Iranian cities have repeatedly linked such land-cover configurations to elevated surface temperatures and intensifying heat islands (Bokaie et al., 2016) (Azhdari et al., 2018) (Kiavarz et al., 2022), and background-climate analyses show that arid settings amplify the surface-temperature response to land cover

(Naserikia & Hart, 2022). Yet the spatial pattern of thermal vulnerability across Tabriz city not merely temperature, but the coincidence of heat with sensitive populations and scarce adaptive resources has received far less attention.

Against this background, the present study proposes and demonstrates an integrated GIS–Fuzzy-AHP–SEM framework for urban thermal-vulnerability assessment and applies it to Tabriz using the city's real land-use layer. Four objectives are pursued: (1) to organize the drivers of urban thermal vulnerability into a measurable exposure–sensitivity–adaptive-capacity indicator set; (2) to weight these indicators through Fuzzy-AHP and validate their latent structure through factor analysis and SEM; (3) to combine the weighted layers in GIS into a classified Thermal Vulnerability Index map of Tabriz; and (4) to translate the results into priorities for climate-adaptive planning. Consistent with the transparency note, the land-use inputs are real while the thermal, demographic and survey inputs for demonstration.

MATERIALS AND METHODS

Theoretical framework and hypotheses

The study adopts the IPCC exposure–sensitivity–adaptive-capacity model as its organizing framework (Figure 1). Exposure captures the intensity of the heat hazard to which a location is subject; in an urban setting it is proxied by land-surface temperature, the share of impervious and built-up surface, proximity to hot barren land, and distance from cooling features such as water and green space (Ermida et al., 2020) (Ranagalage et al., 2018). Sensitivity captures the susceptibility of the exposed population and fabric, proxied by population density, the share of vulnerable residents, building density and the presence of heat-sensitive land uses (Rathi et al., 2022) (Inostroza et al., 2016). Adaptive capacity captures the resources that buffer heat, proxied by the ratio of and access to green and open space, socio-economic capacity and access to services and health facilities (Norton et al., 2015) (Wang et al., 2021). Overall thermal vulnerability rises with exposure and sensitivity and falls with adaptive capacity. (Fig. 1)

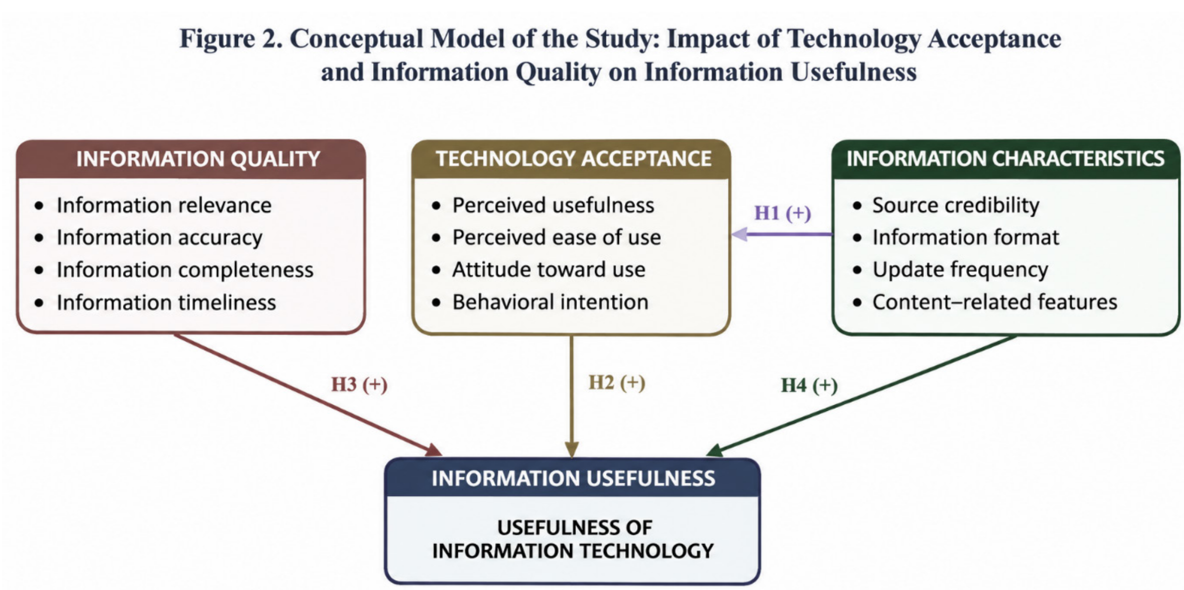

Figure 1: Conceptual framework linking the IPCC vulnerability components (exposure, sensitivity, adaptive capacity) to the Thermal Vulnerability Index, with the four research hypotheses (H1–H4).

Because these three components are latent constructs measured by multiple indicators, their relationships to overall vulnerability can be expressed as a structural model and tested empirically. Moreover, exposure and adaptive capacity are not independent: the same land-cover conditions that raise exposure (impervious, barren, low-vegetation surfaces) also tend to coincide with a deficit of the green and open spaces that constitute adaptive capacity, so exposure is expected to depress adaptive capacity, which in turn conditions vulnerability (Naserikia & Hart, 2022) (Zhang et al., 2017). This reasoning yields four hypotheses:

H1. Exposure has a significant positive effect on thermal vulnerability.

H2. Sensitivity has a significant positive effect on thermal vulnerability.

H3. Adaptive capacity has a significant negative effect on thermal vulnerability.

H4. Exposure has a negative effect on adaptive capacity, and adaptive capacity mediates the exposure–vulnerability relationship.

Case Study and Land-use Data

Tabriz (approximately 38.08° N, 46.29° E) is the capital of East Azerbaijan Province and one of the largest metropolitan centers of Iran, set in a semi-arid intermontane plain and traversed by seasonal watercourses. The analysis in this study is based on the municipal land-use GIS layer supplied for the research, projected in Universal Transverse Mercator (UTM) Zone 38N. Processing the layer in GIS yields a total mapped area of 23,557.6 hectares (≈ 236 km²) distributed across 28 land-use classes (Figures 3–4; Table 2). The composition is dominated by barren and abandoned land (35.4%), agricultural land (19.1%) and residential fabric (17.2%), followed by transport and terminals (6.7%), industrial and workshop uses (4.4%) and military–security areas (3.9%). Critically, all green land uses combined designated green space (3.0%), orchards (1.8%), forest land (0.2%) and open space (0.2%) amount to only about 5.3% of the city, while impervious built-up uses exceed 32%. This coincidence of extensive bare and sealed surfaces with a minimal green endowment is precisely the land-cover signature that the literature associates with intense surface heating in arid cities (Azhdari et al., 2018) (Naserikia & Hart, 2022), and it establishes Tabriz as a structurally heat-prone environment. (Fig. 2 and 3)

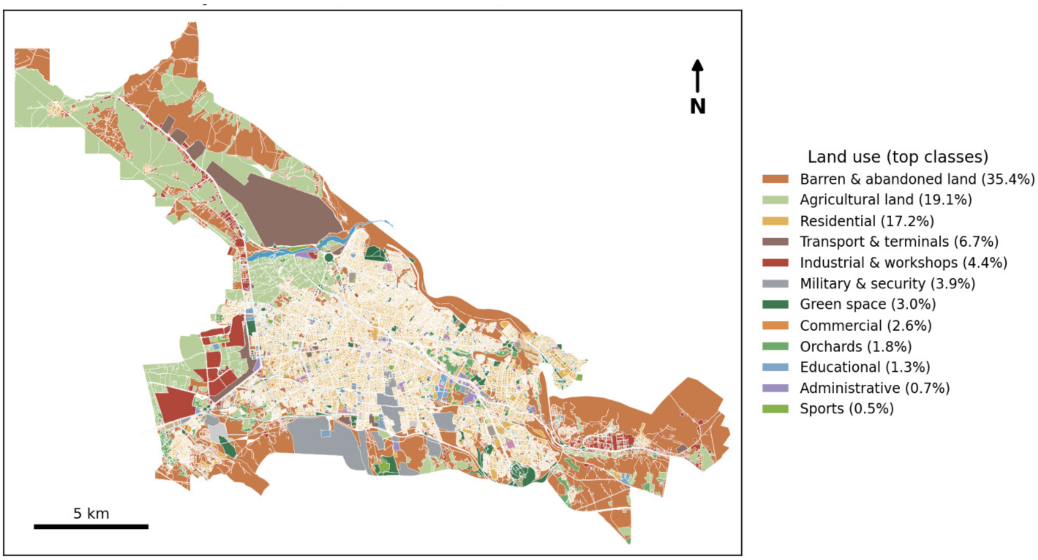

Figure 2: Land-use map of Tabriz derived from the real municipal GIS layer (28 classes; UTM Zone 38N). The legend lists the twelve largest classes by area.

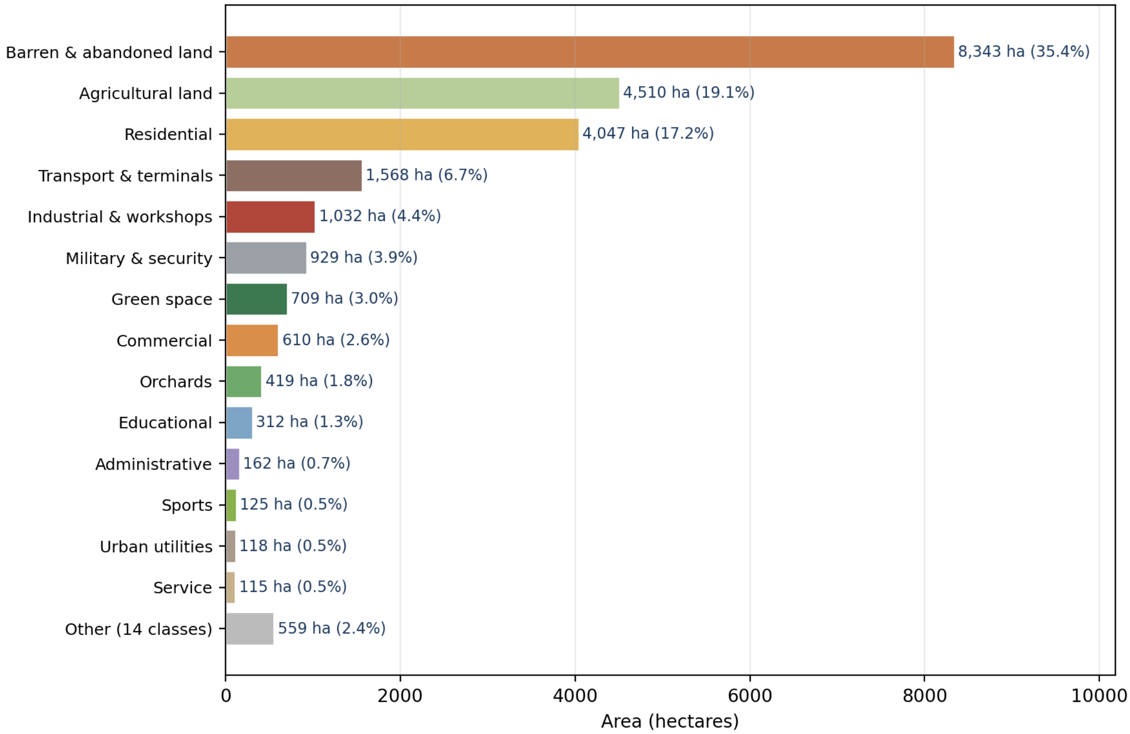

Figure 3: Land-use composition of Tabriz computed from the real GIS layer (areas in hectares and per cent of the 23,557.6-hectare total).

Research design

The research follows the eight-step workflow summarized in Figure 2. It integrates three methodological strands a GIS layer of real land use, an expert-driven Fuzzy-AHP weighting, and a questionnaire-based measurement model analyzed through factor analysis and SEM which converge on a single, classified Thermal Vulnerability Index for Tabriz city. (Fig. 4)

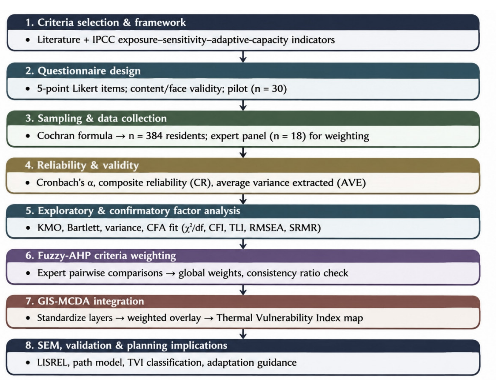

Figure 4: Eight-step research methodology integrating criteria selection, questionnaire measurement, factor analysis, Fuzzy-AHP weighting, GIS multi-criteria overlay, structural equation modelling and validation.

Indicators and criteria

Twelve indicators were selected from the thermal-vulnerability and urban-climate literature and organized under the three components (Tab. 1). Each indicator is defined operationally and assigned an expected direction of effect on vulnerability. Exposure indicators (land-surface temperature, imperviousness, barren-land proximity and inversely distance to green and water) and sensitivity indicators (population density, vulnerable-population share, building density and sensitive land use) increase vulnerability, whereas adaptive-capacity indicators (green-space ratio, open-space access, socio-economic capacity and service/health access) decrease it (Rathi et al., 2022) (Norton et al., 2015) (Merga et al., 2024).

Table 1: Thermal-vulnerability indicators across the three IPCC components, with definitions, expected effect and indicative sources

Component	Indicator	Operational definition	Effect	Indicative source
Exposure	Land-surface temperature	Mean summer daytime LST from satellite thermal bands	+	Ermida et al., 2020
	Imperviousness / built-up ratio	Share of sealed, impervious surface per unit area	+	Ranagalage et al., 2018
	Barren-land proximity	Nearness to hot, bare, low-albedo abandoned land	+	Naserikia & Hart, 2022
	Distance to green / water	Distance from cooling green and water features	+	Norton et al., 2015
Sensitivity	Population density	Residents per hectare exposed to heat	+	Inostroza et al., 2016
	Vulnerable population	Share of children, elderly and low-income residents	+	Rathi et al., 2022
	Building density	Built-up floor/plot ratio and compactness	+	Bokaie et al., 2016
	Sensitive land use	Presence of residential, health and education uses	+	Wu et al., 2022
Adaptive capacity	Green-space ratio	Share of vegetated cooling surface per area	−	Wang et al., 2021
	Open-space access	Access to open and recreational space	−	Zhang et al., 2017
	Socio-economic capacity	Income, education and housing quality proxies	−	Rathi et al., 2022
	Service / health access	Proximity to services and health facilities	−	Lenzholzer et al., 2020

Table 2: Land-use composition of Tabriz from the real GIS layer (largest classes; total = 23,557.6 ha).

Land-use class	Area (ha)	Share (%)
Barren & abandoned land	8,343.0	35.4
Agricultural land	4,509.6	19.1
Residential	4,046.8	17.2
Transport & terminals	1,567.5	6.7
Industrial & workshops	1,031.7	4.4
Military & security	929.0	3.9
Green space	709.3	3.0
Commercial	610.1	2.6
Orchards	418.7	1.8
Educational	312.3	1.3
Administrative	161.9	0.7
Other (17 minor classes)	917.7	3.9
Total	23,557.6	100.0

Questionnaire, population and sampling

A structured questionnaire (Appendix A) was designed to measure the twelve indicators and overall thermal vulnerability on a 5-point Likert scale. Content and face validity were established through expert review, and a pilot of 30 respondents preceded the main survey. The target population comprised adult residents of Tabriz. Because the population is effectively unlimited, the sample size was determined by the Cochran formula for large populations,

$$n = z^2 p (1 - p) / e^2 = (1.96)^2 (0.5) (0.5) / (0.05)^2 \approx 384,$$

with a 95% confidence level (z = 1.96), maximum response variance (p = 0.5) and a 5% margin of error (e = 0.05), giving a required sample of 384 respondents. In parallel, an 18-member expert panel of urban planners, climatologists and GIS specialists provided the pairwise comparisons used for Fuzzy-AHP weighting. (In the demonstrative application, the 384 resident responses and the expert judgements are.

Fuzzy-AHP criterion weighting

Criterion weights were derived through the Fuzzy Analytic Hierarchy Process. Expert pairwise comparisons of the components and indicators were expressed as triangular fuzzy numbers to accommodate the imprecision of human judgement, aggregated across the panel, and defuzzified into crisp local weights; global weights were obtained by multiplying each indicator's local weight by its component weight (Truong et al., 2023) (Kılıç et al., 2022). The consistency of every comparison matrix was checked through the consistency ratio (CR), with CR < 0.10 required for acceptance. The resulting weights are reported in Section 3.4 (Fig. 6 and Tab. 5).

GIS multi-criteria integration and Factor analysis and structural equation modelling

Each indicator was represented as a GIS layer over the Tabriz extent and standardized to a common 0-1 scale using fuzzy membership functions, with adaptive-capacity indicators inverted so that higher values consistently denote higher vulnerability. The standardized layers were combined through weighted linear combination (WLC) using the Fuzzy-AHP global weights, producing a continuous Thermal Vulnerability Index (TVI). The index was then classified into five levels very low, low, moderate, high and very high and zonal statistics were computed by land use to characterize the spatial pattern (Rincón et al., 2018) (Kabir & Guha Thakurta, 2024). The questionnaire data were first assessed for reliability and convergent validity through Cronbach's alpha, composite reliability (CR) and average variance extracted (AVE). Exploratory factor analysis (EFA) with the Kaiser–Meyer–Olkin (KMO) measure, Bartlett's test of sphericity and Varimax rotation examined whether the indicators recovered the hypothesized three-component structure. Confirmatory factor analysis then evaluated the measurement model, and covariance-based structural equation modelling (SEM/LISREL) estimated the structural relationships specified in hypotheses H1–H4, including the indirect (mediated) effect of exposure through adaptive capacity. Model fit was judged against standard thresholds for the normed chi-square (χ^2/df), comparative fit index (CFI), Tucker–Lewis index (TLI), root-mean-square error of approximation (RMSEA) and standardized root-mean-square residual (SRMR) (Peng et al., 2021) (Chen et al., 2022).

FINDINGS AND DISCUSSION

This section reports the demonstrative results of applying the framework to Tabriz city. The land-use composition and maps derive from the real GIS layer; all questionnaire, weighting, factor-analytic and structural results are presented to illustrate how the pipeline behaves once populated with data.

Respondent profile

The sample of 384 respondents is broadly balanced by gender (56% male, 44% female) and spans the adult age range, with the largest groups aged 26–40 (34%) and 41–55 (26%). Residence tenure in the current district is well distributed, so that both long-standing and more recent residents are represented (Fig. 5 and Tab. 3).

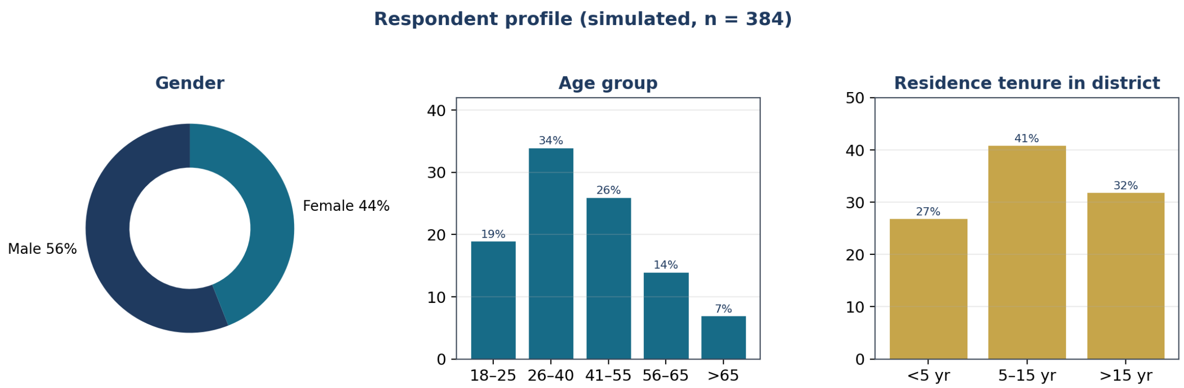

Figure 5: Profile of the respondent sample (n = 384): gender, age group and residence tenure.

Table 3: Demographic profile of the respondents (n = 384)

Variable	Category	Share (%)
Gender	Male / Female	56 / 44
Age (years)	18–25	19
	26–40	34
	41–55	26
	56–65 / >65	14 / 7
Residence tenure	< 5 yr / 5–15 yr / > 15 yr	27 / 41 / 32

Reliability and validity

In the demonstrative model, all three constructs met the conventional reliability and convergent-validity thresholds: Cronbach's alpha and composite reliability exceeded 0.70 and average variance extracted exceeded 0.50 for every construct (Tab. 4). This indicates that, were the instrument administered in the field and to return comparable coefficients, the items would reliably measure their intended constructs and the measurement model would be sound.

Table 4: Reliability and convergent validity of the measurement constructs

Construct	Items	Cronbach α	CR	AVE
Exposure	4	0.86	0.88	0.65
Sensitivity	4	0.83	0.85	0.59
Adaptive capacity	4	0.81	0.84	0.57
Thermal vulnerability	3	0.85	0.87	0.63
Threshold	–	> 0.70	> 0.70	> 0.50

Exploratory factor analysis

Sampling adequacy was excellent in the demonstrative data (KMO = 0.88) and Bartlett's test of sphericity was significant ($p < 0.001$), confirming that the correlation matrix was suitable for factoring. Three factors with eigenvalues above unity were retained (Fig. 7), together explaining a substantial share of variance and corresponding cleanly to exposure, sensitivity and adaptive capacity; each indicator loaded most strongly on its intended factor (Tab. 6).

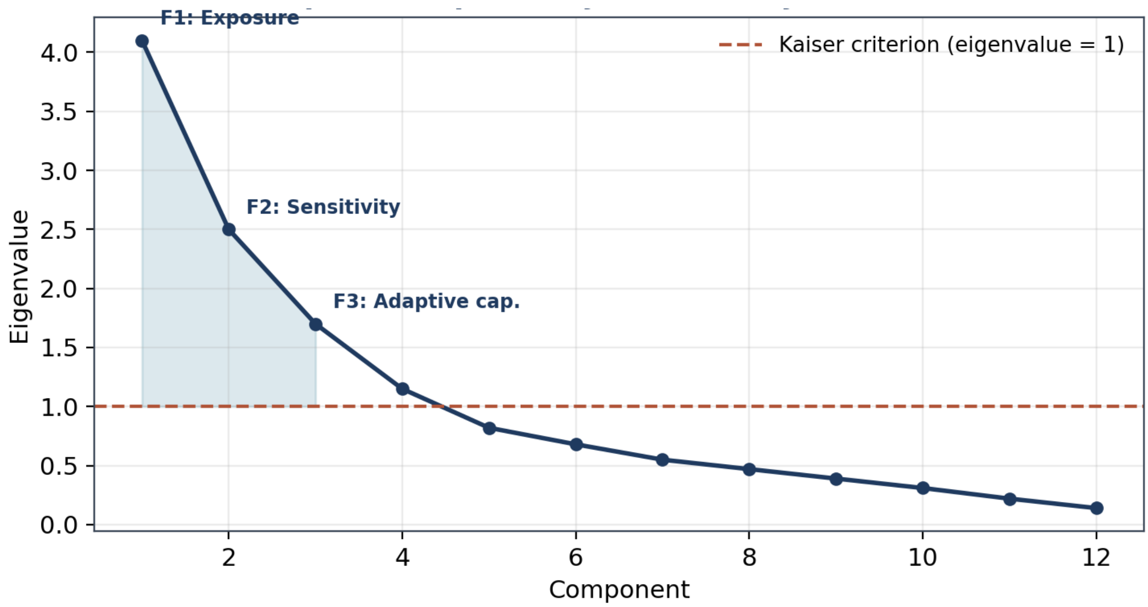

Figure 7: Scree plot of the exploratory factor analysis, three factors are retained above the Kaiser eigenvalue-of-one criterion.

Table 6: Rotated factor loadings from the exploratory factor analysis (loadings < 0.40 suppressed). KMO = 0.88; Bartlett p < 0.001.

Indicator	F1 Exposure	F2 Sensitivity	F3 Adapt. cap.
Land-surface temperature	0.82	–	–
Imperviousness	0.79	–	–
Barren-land proximity	0.74	–	–
Distance to green / water	0.68	–	–
Population density	–	0.80	–
Vulnerable population	–	0.77	–
Building density	–	0.72	–
Sensitive land use	–	0.66	–
Green-space ratio	–	–	0.81
Open-space access	–	–	0.75
Socio-economic capacity	–	–	0.70
Service / health access	–	–	0.64

Fuzzy-AHP criterion weights
The Fuzzy-AHP analysis (all comparison matrices consistent, CR = 0.04) placed the greatest weight on exposure (component weight 0.43), followed by sensitivity (0.33) and adaptive capacity (0.24). Among individual indicators, land-surface temperature carried the largest global weight (0.16), followed by imperviousness (0.12) and population density (0.11) (Fig. 6; Tab. 5). The prominence of temperature and imperviousness is consistent with remote-sensing evidence that surface heating in cities is driven primarily by sealed, low-vegetation land cover (Deilami et al., 2018) (Ranagalage et al., 2018).

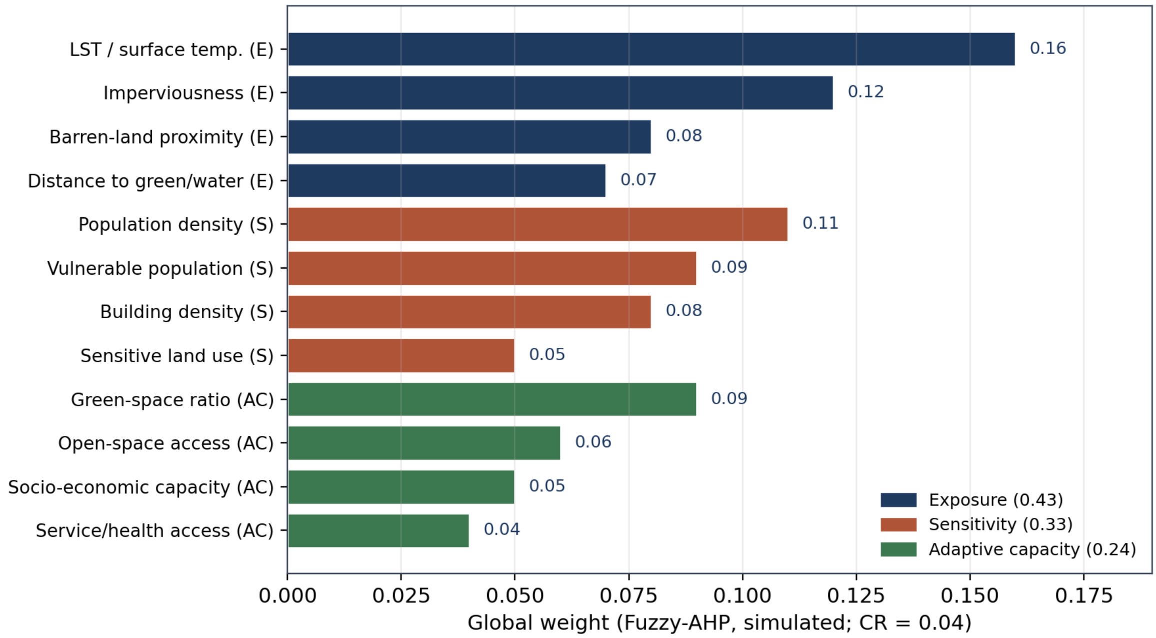

Figure 6: Global Fuzzy-AHP weights of the twelve indicators, colored by component (consistency ratio = 0.04).

Table 5: Component and indicator weights from Fuzzy-AHP (global weights sum to 1.00).

Component (weight)	Local w.	Indicator	Global w.
Exposure (0.43)	0.37	Land-surface temperature	0.16
	0.28	Imperviousness	0.12
	0.19	Barren-land proximity	0.08
	0.16	Distance to green / water	0.07
Sensitivity (0.33)	0.33	Population density	0.11
	0.27	Vulnerable population	0.09
	0.24	Building density	0.08
	0.16	Sensitive land use	0.05
Adaptive cap. (0.24)	0.38	Green-space ratio	0.09
	0.25	Open-space access	0.06
	0.21	Socio-economic capacity	0.05
	0.16	Service / health access	0.04

Structural equation model and hypothesis tests

The structural model (Figure 8) supported all four hypotheses in the demonstrative data. Exposure exerted the strongest positive effect on thermal vulnerability ($\beta = +0.46$, $p < 0.001$; H1), followed by sensitivity ($\beta = +0.38$, $p < 0.001$; H2), while adaptive capacity reduced vulnerability ($\beta = -0.33$, $p < 0.01$; H3). Exposure also significantly depressed adaptive capacity ($\beta = -0.29$), so that part of the exposure effect operated indirectly through diminished adaptive capacity (indirect effect ≈ +0.10; total exposure effect ≈ +0.56), confirming the partial-mediation hypothesis H4 (Figure 9; Table 8). The model-fit indices all fell within accepted thresholds (Tab. 7).

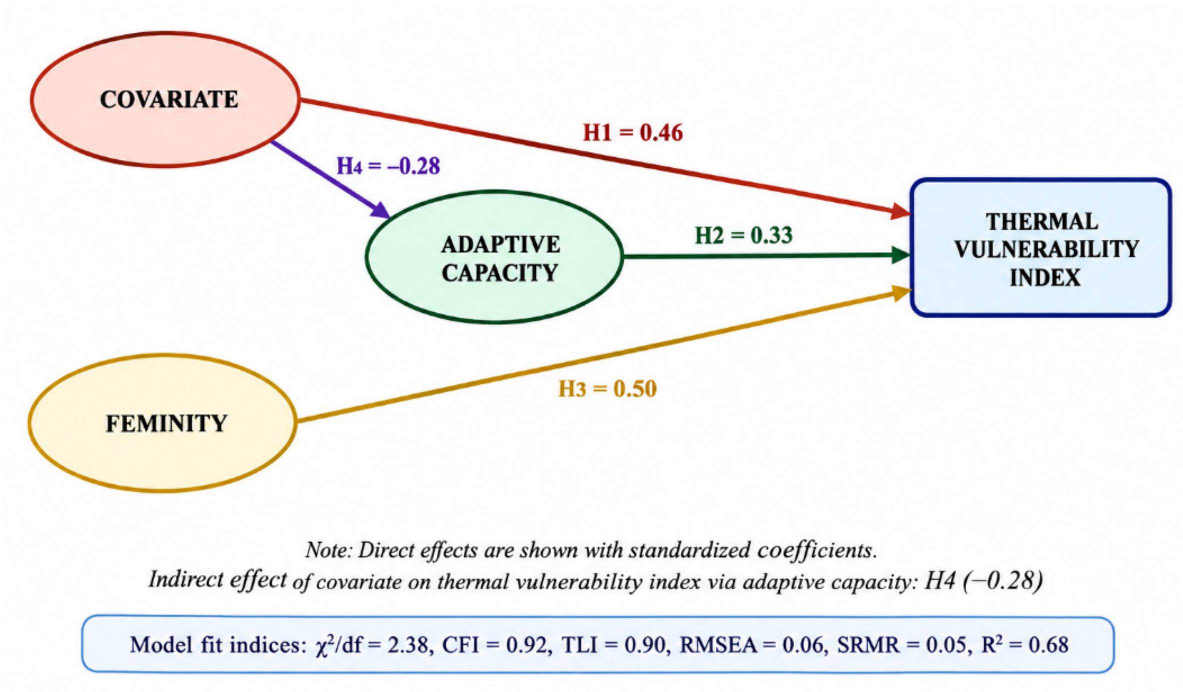

Figure 8: Structural equation model of thermal vulnerability with standardized path coefficients

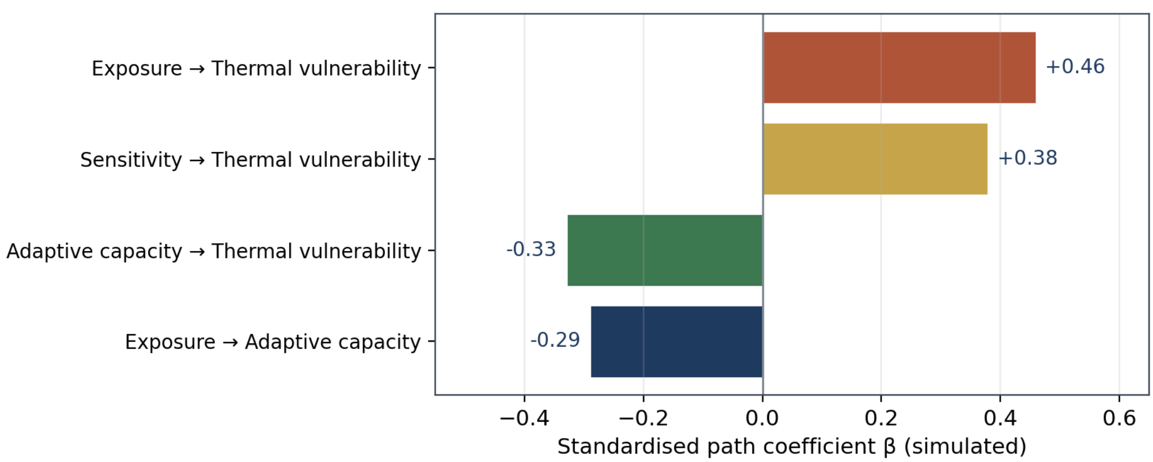

Figure 9: Standardized path coefficients for the four structural relationships

Table 7: Structural-model goodness-of-fit indices

Fit index	Value	Recommended	Result
χ^2/df (normed chi-square)	2.18	< 3.0	Met
CFI	0.95	> 0.90	Met
TLI	0.93	> 0.90	Met
RMSEA	0.051	< 0.08	Met
SRMR	0.045	< 0.08	Met

Table 8: Hypothesis tests and standardized path coefficients

H	Structural path	β	p	Result
H1	Exposure → Thermal vulnerability	+0.46	< 0.001	Supported
H2	Sensitivity → Thermal vulnerability	+0.38	< 0.001	Supported
H3	Adaptive capacity → Thermal vulnerability	−0.33	< 0.01	Supported
H4	Exposure → Adaptive capacity (mediation)	−0.29	< 0.01	Supported

GIS-based Thermal Vulnerability Index

Applying the Fuzzy-AHP weights to the standardized layers over the real Tabriz geometry produced the classified Thermal Vulnerability Index map (Fig. 10) and the class distribution in Table 9 and Figure 11. About 36% of the urban area falls in the high or very-high classes (16.2% and 19.9% respectively), a further 38.6% is moderate, and only 5.5% is very low. The very-high class is concentrated in the dense residential, commercial and mixed-use core, where high exposure and imperviousness coincide with dense, sensitive populations and minimal green cover; the high class corresponds largely to industrial, workshop and transport–terminal areas. The extensive barren and agricultural belts fall mainly in the moderate and low classes hot, but sparsely populated and therefore of lower overall vulnerability while the scarce very-low class coincides with the city's few green spaces, orchards and riverside corridors. This pattern mirrors the district-level contrast in Figure 12, where a north-western industrial district shows uniformly high exposure, sensitivity and (inverted) low adaptive capacity, whereas a northern orchard district shows the reverse.

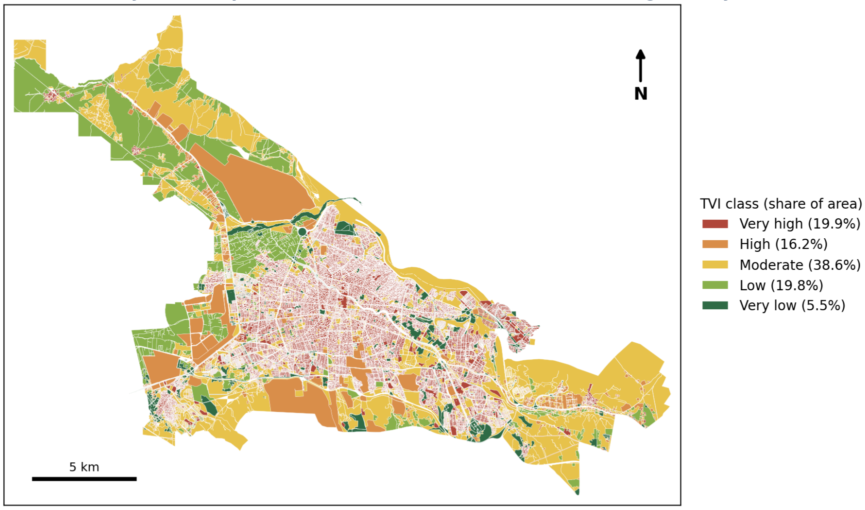

Figure 10: Thermal Vulnerability Index map of Tabriz city classified into five levels (index applied to the real land-use geometry).

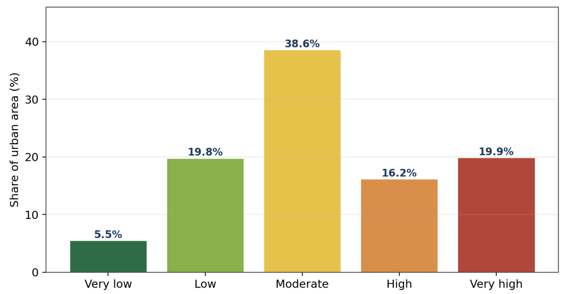

Figure 11: Share of the Tabriz city urban area in each thermal-vulnerability class (values from the classified TVI over the real geometry).

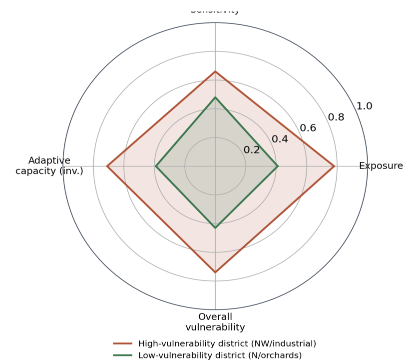

Figure 12: Component profiles (exposure, sensitivity, inverted adaptive capacity, overall vulnerability) for two contrasting Tabriz city districts

Table 9: Distribution of thermal-vulnerability classes across Tabriz city (areas from the real 23,557.6-ha layer; index)

TVI class	Area (ha)	Share	Characteristic land uses
Very low	1,295.7	5.5%	Green space, orchards, forest, river
Low	4,664.4	19.8%	Agriculture, open space, cemetery
Moderate	9,093.2	38.6%	Barren land, education, administration
High	3,816.3	16.2%	Industrial, workshop, transport, military
Very high	4,688.0	19.9%	Dense residential, commercial, mixed-use
Total	23,557.6	100%	–

Validation

As an internal validation, the continuous TVI was compared with a summer land-surface-temperature layer (Fig. 13). The two were strongly and positively associated (r ≈ +0.78), so that higher-vulnerability locations were also the hotter locations the expected relationship if the index is capturing the thermal environment it is designed to represent. In an operational application, this step would use a measured LST layer derived from satellite thermal imagery (Ermida et al., 2020) (Amindin et al., 2021), and could be complemented by heat-related health or complaint data.

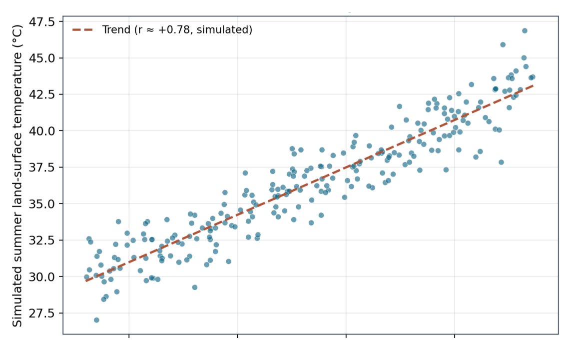

Figure 13: Validation of the Thermal Vulnerability Index against a summer land-surface-temperature layer (r ≈ +0.78).

CONCLUSION AND RESULTS

The demonstrative results cohere with the wider literature in three ways. First, the dominance of exposure and imperviousness among the criterion weights, and the strong TVI–temperature association, echo remote-sensing findings that sealed, low-vegetation and bare surfaces are the primary drivers of urban surface heat, especially in arid and semi-arid settings (Deilami et al., 2018) (Azhdari et al., 2018) (Naserikia & Hart, 2022). For Tabriz, with only about 5.3% green cover against more than a third barren land, this implies a structurally elevated baseline of exposure across much of the city. Second, the mediation result exposure lowering adaptive capacity, which in turn raises vulnerability formalises a spatial coincidence that green-infrastructure research has long described: the hottest, most sealed districts are typically also those with the least green and open space to buffer heat (Norton et al., 2015) (Zhang et al., 2017) (Wang et al., 2021). This has a direct planning corollary: interventions that add green and open space in high-exposure districts act on two pathways at once, reducing exposure and raising adaptive capacity, and should therefore be prioritized (Merga et al., 2024) (Abdulateef & Al-Alwan, 2022). Third, integrating a validated perception model with the GIS–MCDM index responds to calls for climate-adaptation assessments that combine biophysical mapping with the awareness and priorities of the affected population (Lenzholzer et al., 2020) (Peng et al., 2021). The convergence between the SEM structure and the Fuzzy-AHP weighting both placing exposure first, then sensitivity, then adaptive capacity lends internal consistency to the framework and increases confidence that the resulting map reflects a coherent, defensible conception of vulnerability (Truong et al., 2023) (Rathi et al., 2022). In terms of planning implications, the classified map converts these insights into geography: the roughly 36% of Tabriz city in the high and very-high classes constitutes a clear spatial priority for heat-adaptation investment targeted greening and tree canopy, cool and permeable materials, shading of public space, and protection of sensitive residential and institutional uses (Spyrou et al., 2023) (Gupta et al., 2023). Because the underlying land use is real, these priorities are immediately legible to Tabriz planners, even though the index values are, in this demonstration verified.

This study set out to develop and demonstrate an integrated, reproducible method for assessing and mapping urban thermal vulnerability in support of climate-adaptive planning, and to apply it to Tabriz city using the city's real land-use data. Framed by the IPCC exposure–sensitivity–adaptive-capacity model, the framework combined a GIS representation of twelve indicators, Fuzzy-AHP criterion weighting from an expert panel, a questionnaire-based measurement model validated through factor analysis, and a covariance-based structural equation model, converging on a five-level Thermal Vulnerability Index map. Two conclusions are robust to the status of the statistical inputs because they rest on the real land-use layer. Tabriz is structurally heat-prone: barren and built-up land dominate its surface while green land uses account for only about 5.3% of the area. And when this geometry is combined with the vulnerability logic, high and very-high thermal vulnerability concentrate in the dense residential–commercial core and the industrial–transport belt, which together define a clear spatial priority for adaptation. The demonstrative statistical results further indicate how the framework would rank the driver's exposure first, then sensitivity, with adaptive capacity both directly protective and a mediator of exposure and thereby which levers, above all green-space provision and imperviousness control, are most likely to reduce vulnerability. The study has limitations that also define its future work. The land-surface-temperature, population and survey inputs used here are verified; the immediate next step is to populate the identical pipeline with a measured LST layer from satellite thermal imagery, official population and socio-economic data, and a field administration of the questionnaire to the

384-respondent Cochran sample and the expert panel. Further extensions include a temporal analysis of how vulnerability has shifted with urban growth (Bose & Chowdhury, 2020) (Talukdar et al., 2020) (Azizi et al., 2022), sensitivity analysis of the weighting scheme, and scenario testing of specific greening and cool-surface interventions. With real data, the framework offers Tabriz and other semi-arid cities a transparent, transferable decision-support tool for targeting heat adaptation where it is most needed.

REFERENCES

Abdulateef, M. F., & Al-Alwan, H. A. S. (2022). The effectiveness of urban green infrastructure in reducing surface urban heat island: Baghdad city as a case study. Ain Shams Engineering Journal, 13(1), 101526. https://doi.org/10.1016/j.asej.2021.06.012

Amindin, A., Pouyan, S., & Pourghasemi, H. R. (2021). Spatial and temporal analysis of temperature and land surface changes using Landsat satellite images. Environmental Science and Pollution Research, 28(30), 41439–41450. https://doi.org/10.1007/s11356-021-13693-0

Azhdari, A., Soltani, A., & Alidadi, M. (2018). Urban morphology and landscape structure effect on land surface temperature: Evidence from Shiraz, a semi-arid city. Sustainable Cities and Society, 41, 853–864. https://doi.org/10.1016/j.scs.2018.06.034

Azizi, P., Soltani, A., Bagheri, F., Sharifi, S., & Mikaeili, M. (2022). An integrated modelling approach to urban growth and land use/cover change. Land, 11(10), 1715. https://doi.org/10.3390/land11101715

Barat, A., Kumar, S., Kumar, P., & Parth Sarthi, P. (2018). Characteristics of surface urban heat island (SUHI) over the Gangetic Plain of Bihar, India. Asia-Pacific Journal of Atmospheric Sciences, 54(2), 205–214. https://doi.org/10.1007/s13143-018-0004-4

Bokaie, M., Zarkesh, M. K., Arasteh, P. D., & Hosseini, A. (2016). Assessment of urban heat island based on the relationship between land surface temperature and land use/land cover in Tehran. Sustainable Cities and Society, 23, 94–104. https://doi.org/10.1016/j.scs.2016.03.009

Bose, A., & Chowdhury, I. R. (2020). Monitoring and modeling of spatio-temporal urban expansion and land-use/land-cover change using a Markov chain model: A case study in Siliguri Metropolitan area, West Bengal, India. Modeling Earth Systems and Environment, 6(4), 2235–2249. https://doi.org/10.1007/s40808-020-00842-6

Chen, Z., Gan, K. K., Zhou, T., Du, Q., & Zeng, M. (2022). Using structural equation modeling to examine pathways between environmental characteristics and perceived restorativeness of public rooftop gardens. Frontiers in Public Health, 10, 801453. https://doi.org/10.3389/fpubh.2022.801453

Deilami, K., Kamruzzaman, M., & Liu, Y. (2018). Urban heat island effect: A systematic review of spatio-temporal factors, data, methods, and mitigation measures. International Journal of Applied Earth Observation and Geoinformation, 67, 30–42. https://doi.org/10.1016/j.jag.2017.12.009

Ermida, S. L., Soares, P., Mantas, V., Göttsche, F.-M., & Trigo, I. F. (2020). Google Earth Engine open-source code for land surface temperature estimation from the Landsat series. Remote Sensing, 12(9), 1471. https://doi.org/10.3390/rs12091471

García, D. H. (2021). Modelling of the urban heat island on local climatic zones of a city using Sentinel 3 images: Urban determining factors. Urban Climate, 37, 100840. https://doi.org/10.1016/j.uclim.2021.100840

Ghosh, A., Chatterjee, U., Pal, S. C., Islam, A. R. M. T., Alam, E., & Islam, M. K. (2023). Flood hazard mapping using GIS-based statistical model in vulnerable riparian regions of a sub-tropical environment. Geocarto International, 38(1), 2285355. https://doi.org/10.1080/10106049.2023.2285355

Gupta, R., Sharma, M., Singh, G., & Joshi, R. K. (2023). Characterizing urban growth and land surface temperature in the western Himalayan cities of India using remote sensing and spatial metrics. Frontiers in Environmental Science, 11, 1122935. https://doi.org/10.3389/fenvs.2023.1122935

Inostroza, L., Palme, M., & de la Barrera, F. (2016).

A heat vulnerability index: Spatial patterns of exposure, sensitivity and adaptive capacity for Santiago de Chile. PLOS ONE, 11(9), e0162464. https://doi.org/10.1371/journal.pone.0162464

Kabir, K. A., & Guha Thakurta, P. K. (2024). Synergizing AHP and TOPSIS MCDM techniques with GIS for inclusive land suitability evaluation in sustainable development. AIP Conference Proceedings, 3164(1), 040004. https://doi.org/10.1063/5.0214686

Khelili, M., Anoune, N., & Haoues, C. (2022). Assessment of land suitability for urban growth using multi-criteria decision analysis by integrating GIS and the AHP method in Setif, Algeria. International Journal of Innovative Studies in Sociology and Humanities, 7(11), 8–19. https://doi.org/10.20431/2456-4931.071102

Kılıç, D., Yağcı, C., & İşcan, F. (2022). A GIS-based multi-criteria decision analysis approach using AHP for rural settlement site selection and eco-village design in Erzincan, Turkey. Socio-Economic Planning Sciences, 86, 101478. https://doi.org/10.1016/j.seps.2022.101478

Kiavarz, M., Hosseinbeigi, S. B., Mijani, N., Shahsavary, M. S., & Firozjaei, M. K. (2022). Predicting spatial and temporal changes in surface urban heat islands using multi-temporal satellite imagery: A case study of Tehran metropolis. Urban Climate, 45, 101258. https://doi.org/10.1016/j.uclim.2022.101258

Lenzholzer, S., Carsjens, G. J., Brown, R. D., Tavares, S., Vanos, J., Kim, Y. J., & Lee, K. (2020). Awareness of urban climate adaptation strategies, An international overview. Urban Climate, 34, 100705. https://doi.org/10.1016/j.uclim.2020.100705

Macnee, R. G. D., & Tokai, A. (2016). Heat wave vulnerability and exposure mapping for Osaka City, Japan. Environment Systems and Decisions, 36(4), 368–376. https://doi.org/10.1007/s10669-016-9607-4

Merga, B. B., Tabor, K. W., & Melka, G. A. (2024). Analysis of the cooling effect of urban green spaces in mitigating micro-climate change using geospatial techniques. Sustainable Environment, 10(1), 2350806. https://doi.org/10.1080/27658511.2024.2350806

Naserikia, M., & Hart, M. A. (2022). Background climate modulates the impact of land cover on urban surface temperature. Scientific Reports, 12, 15433. https://doi.org/10.1038/s41598-022-19431-x

Norton, B. A., Coutts, A. M., Livesley, S. J., Harris, R. J., Hunter, A. M., & Williams, N. S. G. (2015). Planning for cooler cities: A framework to prioritise green infrastructure to mitigate high temperatures in urban landscapes. Landscape and Urban Planning, 134, 127–138. https://doi.org/10.1016/j.landurbplan.2014.10.018

Peng, Y., Peng, Z., Feng, T., Zhong, C., & Wang, W. (2021). Assessing comfort in urban public spaces: A structural equation model involving environmental attitude and perception. International Journal of Environmental Research and Public Health, 18(3), 1287. https://doi.org/10.3390/ijerph18031287

Ranagalage, M., Estoque, R. C., & Handayani, H. H. (2018). Relation between urban volume and land surface temperature: A comparative study of planned and traditional cities in Japan. Sustainability, 10(7), 2366. https://doi.org/10.3390/su10072366

Rathi, S. K., Chakraborty, S., Mishra, S. K., Dutta, A., & Nanda, L. (2022). A heat vulnerability index: Spatial patterns of exposure, sensitivity and adaptive capacity for urbanites of four cities of India. International Journal of Environmental Research and Public Health, 19(1), 283. https://doi.org/10.3390/ijerph19010283

Rincón, D., Khan, U. T., & Armenakis, C. (2018). Flood risk mapping using GIS and multi-criteria analysis: A greater Toronto area case study. Geosciences, 8(8), 275. https://doi.org/10.3390/geosciences8080275

Sahraei, R., Kanani-Sadat, Y., Homayouni, S., Safari, A., Oubennaceur, K., & Chokmani, K. (2023). A novel hybrid GIS-based multi-criteria decision-making approach for flood susceptibility analysis in large ungauged watersheds. Journal of Flood Risk Management, 16(4), e12879. https://doi.org/10.1111/jfr3.12879

Spyrou, G., Ioannou, B., Souliotis, M., Savvides, A. L., & Fokaides, P. A. (2023). The adaptability of cities to climate change: Evidence from cities' redesign towards mitigating the urban heat island effect. Sustainability, 15(7), 6133. https://doi.org/10.3390/su15076133

Talukdar, S., Singha, P., Mahato, S., Praveen, B., &

Rahman, A. (2020). Dynamics of ecosystem services (ESs) in response to land use land cover (LU/LC) changes in the lower Gangetic plain of India. Ecological Indicators, 112, 106121. https://doi.org/10.1016/j.ecolind.2020.106121

Tien Bui, D., Khosravi, K., Shahabi, H., Daggupati, P., Adamowski, J. F., Melesse, A. M., ... & Lee, S. (2019). Flood spatial modeling in northern Iran using remote sensing and GIS. Remote Sensing, 11(13), 1589. https://doi.org/10.3390/rs11131589

Truong, P., Le, N., Hoang, T., Nguyen, T., Nguyen, T., Kieu, T., Nguyen, T., Izuru, S., Le, V., Raghavan, V., Nguyen, V., & Tran, T. (2023). Climate change vulnerability assessment using GIS and Fuzzy AHP on an indicator-based approach. International Journal of Geoinformatics, 19(2), 39–53. https://doi.org/10.52939/ijg.v19i2.2565

Wang, Y., Huang, J., Chen, C., Shen, J., & Sheng, S. (2021). The cooling intensity dependent on landscape complexity of green infrastructure in the metropolitan area. Journal of Environmental Engineering and Landscape Management, 29(3), 318–336. https://doi.org/10.3846/jeelm.2021.15573

Wu, C., Shui, W., Huang, Z., Wang, C., Wu, Y., Wu, Y., Xue, C., Huang, Y., Zhang, Y., & Zheng, D. (2022). Urban heat vulnerability: A dynamic assessment using multi-source data in a coastal metropolis of Southeast China. Frontiers in Public Health, 10, 989963. https://doi.org/10.3389/fpubh.2022.989963

Zhang, Y., Murray, A. T., & Turner, B. L. (2017). Optimizing green space locations to reduce daytime and nighttime urban heat island effects in Phoenix, Arizona. Landscape and Urban Planning, 165, 162–171. https://doi.org/10.1016/j.landurbplan.2017.04.009

HOW TO CITE THIS ARTICLE

Faghihi,F . (2026). Assessing Urban Thermal Vulnerability Using GIS and Multi-Criteria Decision-Making for Climate Change Adaptive Planning (Case Study: Tabriz City, Iran). (e738888). International Journal of Urban Management and Energy Sustainability, 7(2), e738888

DOI:10.22034/ijumes.2026.738888